Surface & Coatings Technology 205 (2010) 2152–2159

Contents lists available at ScienceDirect

Surface & Coatings Technology

journal homepage: www.elsevier.com/locate/surfcoat

Electrodeposition and characterization of Cu–Nb composite coatings

Alain Robin [a,*], Jorge Luiz Rosa [a], Messias Borges Silva [b]

[a] Departamento de Engenharia de Materiais, Escola de Engenharia de Lorena, Universidade de São Paulo, CP 116, 12600-000 Lorena, SP, Brazil
[b] Departamento de Engenharia Química, Escola de Engenharia de Lorena, Universidade de São Paulo, CP 116, 12600-000 Lorena, SP, Brazil

ARTICLE INFO

Article history:
Received 29 June 2010
Accepted in revised form 29 August 2010
Available online 6 September 2010

Keywords:
Copper
Niobium
Electrocomposites
Design of experiments
Characterization

ABSTRACT

Copper coatings containing well-distributed Nb particles were obtained by co-electrodeposition in an acidic sulfate bath. Nb particle concentration in the bath was the most significant factor for the incorporation of Nb particles in copper, followed by stirring rate, whereas current density presented low significance. High Nb particle concentration and low stirring rate led to a higher incorporated Nb particle content. The microhardness of the composite layers was higher than that of pure copper deposits obtained under the same conditions due to copper matrix grain refinement and increased with the increase of both current density and incorporated Nb particle volume fraction. The corrosion resistance of Cu–Nb composites in 0.5 wt.% H_2SO_4 solution at room temperature was higher than that of pure copper and increased with the increase of the Nb content.

© 2010 Elsevier B.V. All rights reserved.

1. Introduction

Solid particles have been incorporated in metallic electrocoatings during electrodeposition in order to improve their properties, specially their mechanical, wear and corrosion resistance [1,2]. The co-electrodeposition consists in electrolyzing a solution containing the metallic salts and the particles in suspension. The amount of incorporated particles, and consequently the composite coating properties are affected by the electrolysis parameters (bath composition, pH, temperature, cathodic current density and stirring rate) and the particle characteristics (type, mean size and concentration in the bath).

The copper electroplates have high electrical and thermal conductivity, good ductility and good corrosion resistance but show low mechanical and wear resistance. In order to improve or modify the properties of copper coatings, particles of ceramic [3–12], metallic or intermetallic [13–15] and polymeric materials [16] were incorporated to copper.

The evolution of the incorporated particle content as a function of electrolysis parameters does not follow a general trend and is highly dependent on the particle characteristics. For example, the variation of the particle content in copper electrocoatings with current density and particle concentration in the bath was shown to be different for Al_2O_3 [5,6] and SiC [17] powders. Moreover, disagreements between published results about the evolution of the incorporated particle fraction were also found for the same type of particles [6,17]. The properties of the composite layers are also dependent on the type of incorporated particles. For example, a higher microhardness when compared to pure copper layers was observed for Cu–Al_2O_3 [6,7,18], Cu–SiC [6], Cu–CeO_2 [12] and Cu–WC [19] composites but a lower microhardness was measured for both Cu–MoS_2 and Cu–C [6] coatings.

To our knowledge attempts to incorporate metallic particles in copper by electrodeposition were only carried out for chromium [13]. The codeposition was performed in an acidic sulfate bath containing suspended Cr powder but due to the dissolution of Cr in sulfuric acid, Cu–Cr–S alloys were obtained instead of Cu–Cr composites. No information is available on the incorporation of metallic Nb powder in copper electrocoatings, but since Nb is stable in sulfuric acid solutions at room temperature, the codeposition seems possible. Cu–Nb composites obtained by melting routes were shown to have high tensile strength when highly cold deformed and thus are promising for systems that require materials with high strength, capacity to dissipate heat and high temperature stability [20].

The aim of the present work was the production of Cu–Nb electrocomposites from acidic sulfate bath and their characterization. The influence of cathodic current density, particle concentration in the bath and stirring rate on the incorporated particle volume fraction and on the characteristics of the coatings (roughness, microstructure, microhardness and corrosion behavior) was analyzed. The properties of the composite coatings were compared with those of pure copper deposits.

2. Experimental procedure

Cu–Nb composite coatings were prepared by co-electrodeposition in an aqueous sulfate bath ($150\ gL^{-1}\ CuSO_4 + 30\ gL^{-1}\ H_2SO_4$) containing suspended Nb particles at room temperature. The Nb

* Corresponding author. Tel.: +55 12 31599915; fax: +55 12 31533006.
E-mail address: alain@demar.eel.usp.br (A. Robin).

0257-8972/$ – see front matter © 2010 Elsevier B.V. All rights reserved.
doi:10.1016/j.surfcoat.2010.08.124

powders were produced in-house by hydrogenation/dehydrogenation process [21]. Nb particles of size lower than 20 μm were separated by sieving using a 625-mesh screen and were used in this work. Their mean size was around 15 μm. The specific area of the Nb powders was 0.4566 m^2/g and their typical chemical composition was 30 wt-ppm Al, 100 wt-ppm Fe, 50 wt-ppm Si, 600–2000 wt-ppm Ta, 6000 wt-ppm O and 2250 wt-ppm N. The microhardness of the Nb particles was 230 ± 15 VHN. The Nb particles were maintained in suspension by magnetic agitation at 240, 400 and 550 rpm stirring rate. The particle concentration in the bath was 10, 30 and 50 gL^{-1}.

The electrodeposition runs were performed on AISI 1020 carbon steel cathodes of 100 mm × 6 mm × 1 mm dimensions, previously ground to a 600 grit finish. During the electrolysis, one cathode was placed at the center of a cylindrical electrolytic copper anode of 40 mm diameter, previously etched in dilute HNO_3. Cathodic current densities of 10, 20 and 30 $mAcm^{-2}$ were applied for 7 h 40 min, 3 h 50 min and 2 h 33 min, respectively, in order to obtain deposits of approximately 100 μm thickness. The values of stirring rate, particle concentration and cathodic current density used in the present study are usual values employed for the electrodeposition of Cu-particles [6,7,11,12,17] and other metal-particles composites.

The effect of current density, particle concentration and stirring rate of the electrolyte on the incorporated particle volume fraction was studied. In order to reduce the number of experiments, a Central Composite Design (CCD) with three factors operating at three levels was used. The factors of control were: (A) cathodic current density, (B) stirring rate and (C) particle concentration in the bath. Each factor had three coded levels which were −1, 0 and +1 and their corresponding values are presented in Table 1. A total of twelve experiments, including four replicates at center point, was designed. The corresponding CCD is also shown in Table 1. The different experiments were performed randomly. ANOVA and response surfaces for incorporated particle volume fraction were used in order to analyze the effect of the factors of control and interactions.

Scanning electron microscopy (SEM-LEO VP-1450) was used to evaluate the coating morphology, the distribution and the amount of incorporated particles. The percentage of incorporated particles in the deposits was determined by image analysis of polished cross-section photomicrographs using the Image Tool 2.0 free software. The analysis was performed on twenty photographs of each coating taken at 1000 times magnification. The mean volume fraction of incorporated particles was calculated from the twenty values obtained.

X-ray diffractometry (XRD) (SIEFERT-DEBYEFLEX 1001, Cu-Kα) was employed for compositional and texture analysis of the coatings.

The roughness of the composite coatings was measured using a surface roughness measuring instrument MITUTOYO SJ 201.

The microindentation hardness of the composite coatings was measured on polished cross-sections using a Vickers microhardness tester (MICROMET 2004) applying a 100 g load during 30 s.

The corrosion behavior of the composite coatings was evaluated in naturally aerated 0.5 M H_2SO_4 solutions at room temperature by impedance spectroscopy and potentiodynamic polarization using a typical three-electrode corrosion cell (working electrode: composite coating; counter electrode: platinum; and reference electrode: saturated calomel electrode — SCE). The coatings were immersed for 1 h in the solutions before impedance and polarization experiments. The impedance measurements were made at an open-circuit potential using a sinusoidal signal of 10 mV amplitude and frequencies in the 0.1 Hz–100 kHz range and the polarization measurements were carried out potentiodynamically at 1 mV s^{-1} sweep rate. The Electrochemical Interface SOLARTRON 1287A and the Frequency Response Analyzer SOLARTRON 1260 A, controlled by the Ecorr/Zplot SOLARTRON 125587S software were used.

The morphological, structural and mechanical characteristics, as well as the corrosion resistance of Cu–Nb electrocomposites were compared to those of pure copper electrocoatings obtained under the same electrolysis conditions.

Table 1
(a) Control factors and their respective levels; (b) Factor settings for CCD and incorporated Nb particle volume fraction measured by image analysis.

(a)

Factor	Low	Intermediate	High
	−1	0	+1
A: Cathodic current density ($mAcm^{-2}$)	10	20	30
B: Stirring rate (rpm)	240	400	550
C: Concentration of Nb particles in the bath (gL^{-1})	10	30	50

(b)

Experiment number	Level of control factor			Incorporated particle volume fraction (%)
	A	B	C	
1	−1	−1	−1	0.66
2	+1	−1	−1	1.29
3	−1	+1	−1	0.76
4	+1	+1	−1	1.12
5	−1	−1	+1	7.35
6	+1	−1	+1	10.91
7	−1	+1	+1	2.27
8	+1	+1	+1	5.46
9	0	0	0	4.46
10	0	0	0	6.05
11	0	0	0	5.55
12	0	0	0	4.40

3. Results and discussion

3.1. Coating morphology, texture and incorporated Nb particle content

X-ray patterns of Fig. 1 show that the electrocoatings obtained in the copper sulfate bath containing suspended Nb particles were crystalline and contained Nb particles. Differences in the intensities of the peaks related to the Nb phase between samples are indicative that the amount of incorporated Nb particles was dependent on experimental conditions. All the XRD peaks were indexed using JCPDS diffraction data [22].

From Fig. 2a and c it is clear that the surface morphology of Cu–Nb composite layers obtained using the same cathodic current density (10 or 30 $mAcm^{-2}$) is similar independent on the values of Nb particle concentration and stirring rate. It is expected that the same occurs for 20 $mAcm^{-2}$. Comparing Fig. 2a, b and c, the smoothest deposits were obtained using the lowest current density but the coatings became coarser and nodules appeared growing at the surface as the cathodic

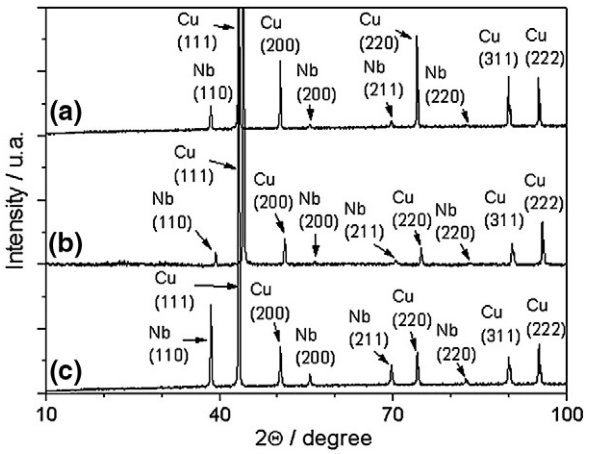

Fig. 1. X-ray patterns of Cu–Nb composite coatings obtained under the following conditions: (a) 10 $mAcm^{-2}$, 240 rpm, 50 gL^{-1}; (b) 20 $mAcm^{-2}$, 400 rpm, 30 gL^{-1}; and (c) 30 $mAcm^{-2}$, 240 rpm, 50 gL^{-1}.

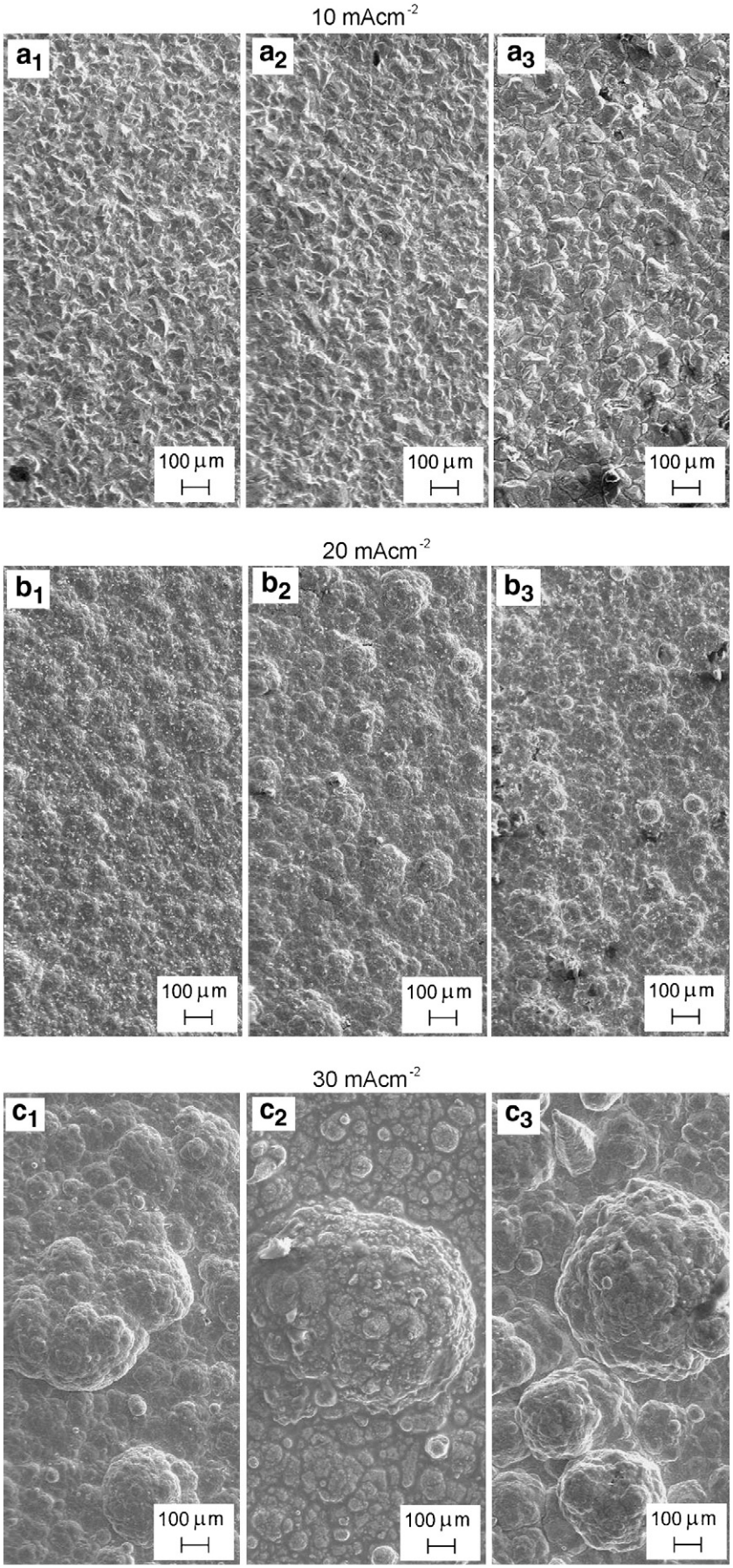

Fig. 2. Surface morphology of Cu–Nb composite coatings obtained using 10 $mAcm^{-2}$: (a_1) 550 rpm, 10 gL^{-1}; (a_2) 240 rpm, 10 gL^{-1}; (a_3) 550 rpm, 50 gL^{-1}; 20 $mAcm^{-2}$: (b_1) 400 rpm, 30 gL^{-1} (exp.9); (b_2) 400 rpm, 30 gL^{-1} (exp. 11); (b_3) 400 rpm, 30 gL^{-1} (exp. 12); 30 $mAcm^{-2}$: (c_1) 240 rpm, 10 gL^{-1}; (c_2) 550 rpm, 10 gL^{-1}; and (c_3) 240 rpm, 50 gL^{-1}.

current density increased. Fig. 2b indicates the reproducibility of surface morphology for coatings performed using the same experimental conditions. Fig. 3 presents the SEM micrograph of a composite coating surface taken at a higher magnification using the back-scatterring electron mode. The Nb particles captured at the surface that appear light (due to a higher atomic number) in contrast to the grey copper matrix are clearly identified.

Fig. 4 shows typical SEM micrographs of the cross-section of composite coatings obtained under different experimental conditions. The Nb particles which have a higher atomic number appear as light spots in the darker copper matrix. The distribution of the Nb particles was homogeneous for all composite coatings but the incorporated particle volume fraction was dependent on experimental conditions. In the case of Fig. 4a, b and c, the incorporated Nb particle volume fraction measured by image analysis was 2.0%, 5.3% and 11.0%, respectively. It can be noted that the size of the embedded particles ranged from 1 to 10 μm. It is probable that larger particles sank before and/or after the impact with the cathode due to their weight and thus were not incorporated in the coatings.

The values of incorporated particle volume fractions in composite coatings obtained under our experimental conditions are reported in Table 1. The Pareto chart of the effect of the factors on the incorporated particle volume fraction is shown in Fig. 5. Pareto chart is a bar chart that displays the relative importance of various factors and puts them in order from the most to the least significant. Fig. 5 indicates with 95% confidence that particle concentration in the bath (C) was the most significant factor, followed by stirring rate (B). The interaction between these factors (B×C) was also significant.

The results of analysis of variance (ANOVA)[23] are presented in Table 2 where:

- SS is the sum of squared deviations from the mean. For n values of y_i and the average value $\overline{y}$

$$SS = \sum_{i=1}^{n} (y_i - \overline{y})^2 \quad (1)$$

- DF is the degree of freedom.
- MS is the mean of squares

$$MS = SS / DF \quad (2)$$

- F is the ratio between the mean of squares effect and the mean of squares error. F test is used to see the significance of each factor (or interaction) on the response variable.

$$F = MS_{effect} / MS_{error} \quad (3)$$

- p is the probability value which gives the degree of confidence at which the factor (or interaction) is significant.

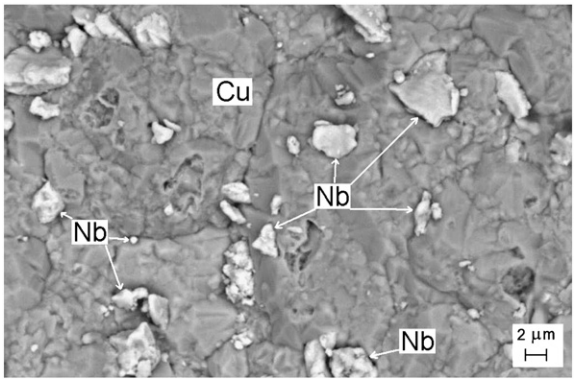

Fig. 3. SEM photograph (backscattering electron mode) of the surface of a Cu–Nb composite coating obtained under the following conditions: 20 $mAcm^{-2}$, 400 rpm, 30 gL^{-1}.

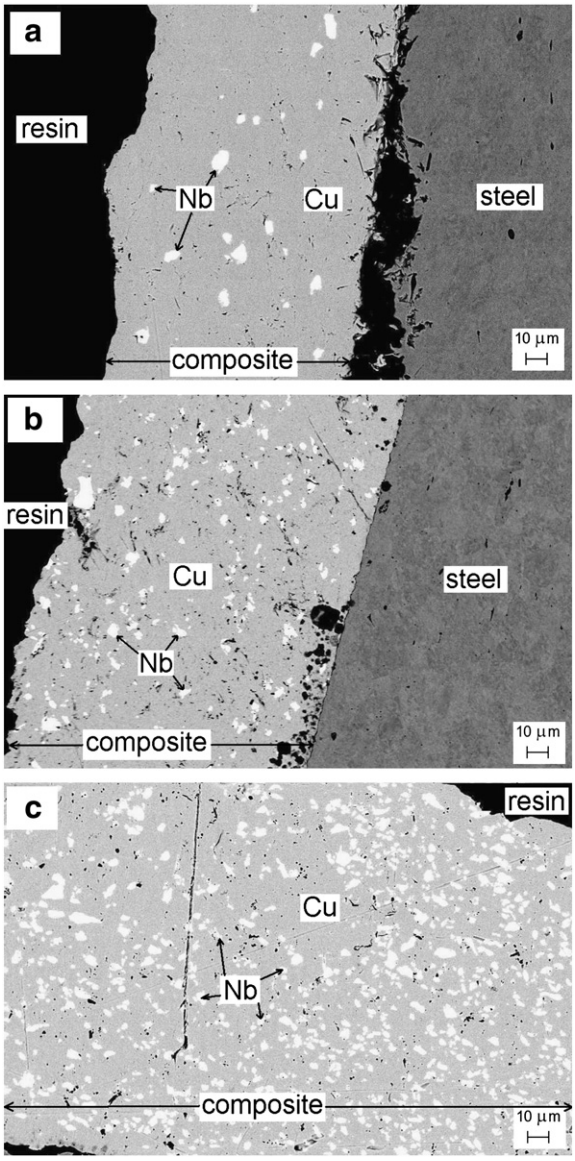

Fig. 4. Cross-sections of Cu–Nb composites obtained under different experimental conditions: (a) 30 $mAcm^{-2}$, 240 rpm, 10 gL^{-1}; (b) 20 $mAcm^{-2}$, 400 rpm, 30 gL^{-1}; and (c) 30 $mAcm^{-2}$, 240 rpm, 50 gL^{-1}.

In ANOVA, for a degree of freedom of 1 for the numerator (effect) and 5 for the denominator (error), the factor is significant with 95% confidence if F exceeds 6.61, and with 90% confidence for F higher

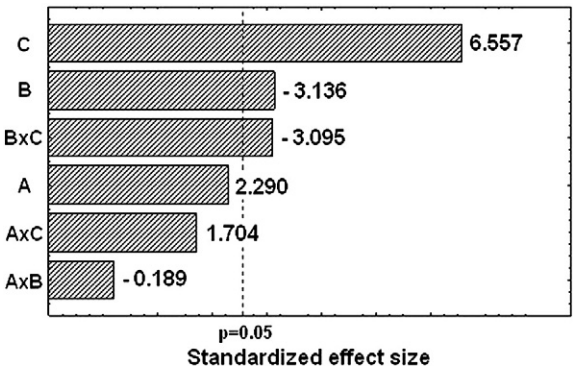

Fig. 5. Pareto chart of the effect of factors and interactions on the incorporated Nb particle volume fraction: (A) current density, (B) stirring rate and (C) particle concentration.

Table 2
Analysis of variance of average response of incorporated Nb particle volume fraction.

	SS*	DF§	MS#	F$	p
(A) Cathodic current density	7.488	1	7.488	5.244	0.071
(B) Stirring rate	14.045	1	14.045	9.837	0.026
(C) Nb particle concentration	61.383	1	61.383	42.993	0.001
A×B	0.051	1	0.051	0.036	0.857
A×C	4.147	1	4.147	2.905	0.149
B×C	13.676	1	13.676	9.579	0.027
Error	7.139	5	1.428		
Total SS	107.930	11			

SS*: sum of squares; DF§: degree of freedom.
MS#: mean of squares; F$: F factor.
p: probability value.

than 4.06 [24] or if p-value is lower than 0.05 and 0.1, respectively. Thus, the values of F in the ANOVA of incorporated Nb particle volume fraction (Table 2) confirm the significant effect of particle concentration in the bath (C), followed by stirring rate (B) and (B×C) interaction. Current density (A) is less significant than (C), (B) and (B×C). (A×B) and (A×C) interactions have no significance. A strong interaction between particle concentration and stirring rate has ever been evidenced for Ni based electrocomposites [25].

Fig. 6 shows the response surfaces for incorporated Nb particle volume fraction as a function of current density (A) and stirring rate (B), stirring rate (B) and particle concentration (C), current density (A) and particle concentration (C). The highest amount of incorporated particles was obtained under the following conditions:

- highest current density and lowest stirring rate (Fig. 6a)
- lowest stirring rate and highest particle concentration (Fig. 6b)
- highest current density and highest particle concentration (Fig. 6c).

Thus, the best condition of adjustment of control factors in order to have the greatest incorporated particle volume fraction is current density (A) to the high level (+1), stirring rate (B) to the low level (−1) and particle concentration to the high level (+1). The main effect plot for the amount of incorporated particles (Fig. 7) indicates that particle concentration (C) has more influence, followed by stirring rate (B) and finally current density (A). Moreover, the behavior between the high (+1) and low (−1) levels is not linear for the three factors.

The following reasons could explain the effect of the investigated electrodeposition parameters on the amount of incorporated Nb particles in copper: (i) the relative unsignificance of the current density on the incorporated particle volume fraction could be related to the diffusion control of the copper cation deposition; then, copper deposition rate would be nearly constant independent on current density and the incorporated Nb particle volume fraction would only depend on stirring rate and Nb particle concentration in the bath; (ii) the increase of the incorporated particle volume fraction with increasing particle concentration in the bath is a general trend [6,7,17] and can be explained by the higher number of particles reaching the cathode; nevertheless, it was shown that too high particle concentration increases the chance of collisions between particles and can have the opposite effect on the amount of incorporated particles; and (iii) increasing stirring rate can lead to the removal of freshly adsorbed particles due to collision factor, which would decrease the amount of embedded particles.

Fig. 8a and b shows the evolution of surface roughness of pure copper and Cu–Nb composite coatings as a function of cathodic current density and incorporated particle content, respectively. The roughness of the composite coatings ranged from 1.8 to 6.1 μm and increased with the increase of current density (Fig. 8a). This increase of roughness is related to the nodular growth of the composite coatings observed when current density increases (Fig. 2). Stankovic [6] observed the same trend for the incorporation of Al_2O_3, SiC, MoS_2

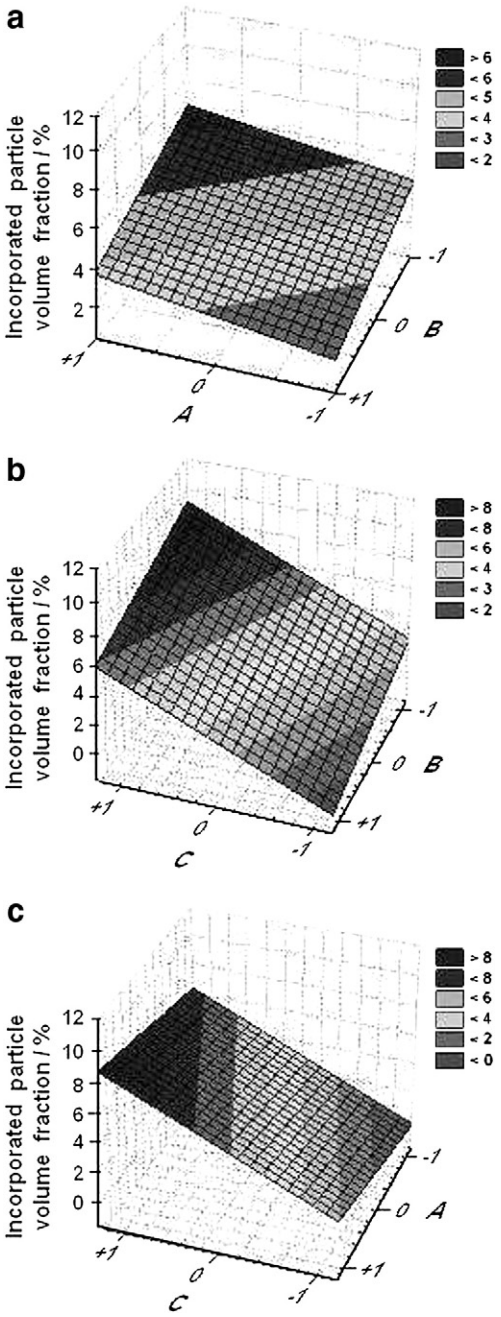

Fig. 6. Response surfaces for incorporated Nb particle volume fraction as a function of (a) current density (A) and stirring rate (B), (b) stirring rate (B) and particle concentration (C) and (c) current density (A) and particle concentration (C).

and C in copper. He also showed that the kind of particles has a greater influence on roughness than the particle size, but did not study the influence of incorporated particle content. As the surface morphology

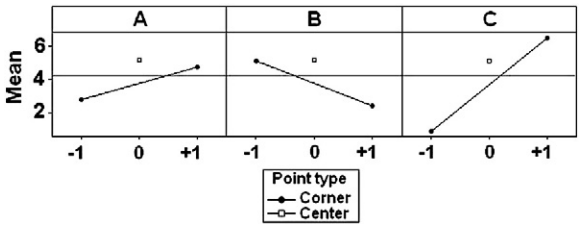

Fig. 7. Main effect plot for the amount of incorporated Nb particles: (A) current density, (B) stirring rate and (C) particle concentration.

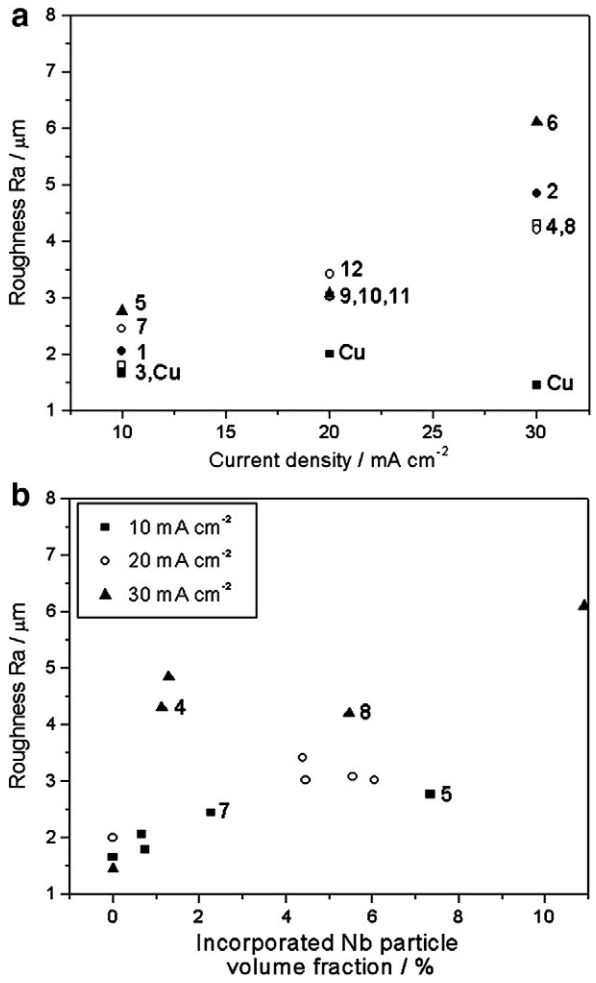

Fig. 8. Ra mean surface roughness of pure copper and Cu–Nb composite coatings as a function of (a) cathodic current density and (b) incorporated Nb particle volume fraction.

of the coatings obtained using the same current density is similar independent on stirring rate and Nb particle concentration (Fig. 2), no noticeable influence of these factors on roughness was found. No defined relation between roughness of the Cu–Nb composite coatings and incorporated Nb particle content can be also deduced from the present results (Fig. 8b). Indeed, the coatings obtained using 10 $mAcm^{-2}$ current density and corresponding to experiments no. 5 and no. 7 contained 7.3 and 2.3% Nb particle volume fraction, respectively, but both deposits presented roughness close to 2.5 µm. The same occurred for coatings obtained using 30 $mAcm^{-2}$ current density: the coatings corresponding to experiments no. 4 and no. 8 presented 1.1 and 5.5% Nb particle content, respectively, but both deposits presented roughness close to 4.2 µm. The pure copper deposits displayed substantial smoothness (roughness lower than 2.0 µm) when compared to the composites and their roughness did not depend significantly on current density.

The orientation index of the (111), (200), (220), (311) and (222) planes of the copper phase was calculated from XRD patterns of Cu–Nb composite coatings (Fig. 1) obtained at 10 (exp. no. 5), 20 (exp. no. 9) and 30 (exp. no. 6) $mAcm^{-2}$ current density from [26]:

$$\text{Orientation index} = (I_{hkl}/\sum I_{hkl})/(I_{ASTM\ hkl}/\sum I_{ASTM\ hkl}) \quad (4)$$

where I_{hkl} and $I_{ASTM\ hkl}$ are the integrated intensities of (hkl) peaks related to the copper phase in the coatings and to copper of random orientation [21], respectively. The same calculation was made for pure copper deposits obtained under the same conditions.

The copper phase was clearly textured in the [110] direction for pure copper coatings obtained using 10 and 20 $mAcm^{-2}$ current densities (Fig. 9a), which means that most copper crystals were oriented with their (220) planes parallel to the surface of the substrate. When Nb particles were co-deposited, the copper grains of the composite matrix did not show anymore preferential orientation, but rather a random orientation (Fig. 9b). The incorporation of Nb particles has perturbed the growth of the copper matrix, probably due to the nucleation of randomly oriented new copper crystals on the embedded Nb particles. Using 30 $mAcm^{-2}$ current density, the copper grains in pure copper coatings were randomly oriented and the incorporation of Nb particles did not lead to any change. The incorporation of TiO_2 to copper electrocoatings [9] was also shown to change the orientation of the copper matrix crystals, whereas the incorporation of Si_3N_4 particles had no effect [27].

3.2. Microhardness

The evolution of microhardness of pure copper and Cu–Nb composite coatings with cathodic current density and incorporated Nb particle content is shown in Fig. 10a and b, respectively.

An increase of microhardness with increasing cathodic current density occurs for both deposits (Fig. 10a) but the microhardness of the

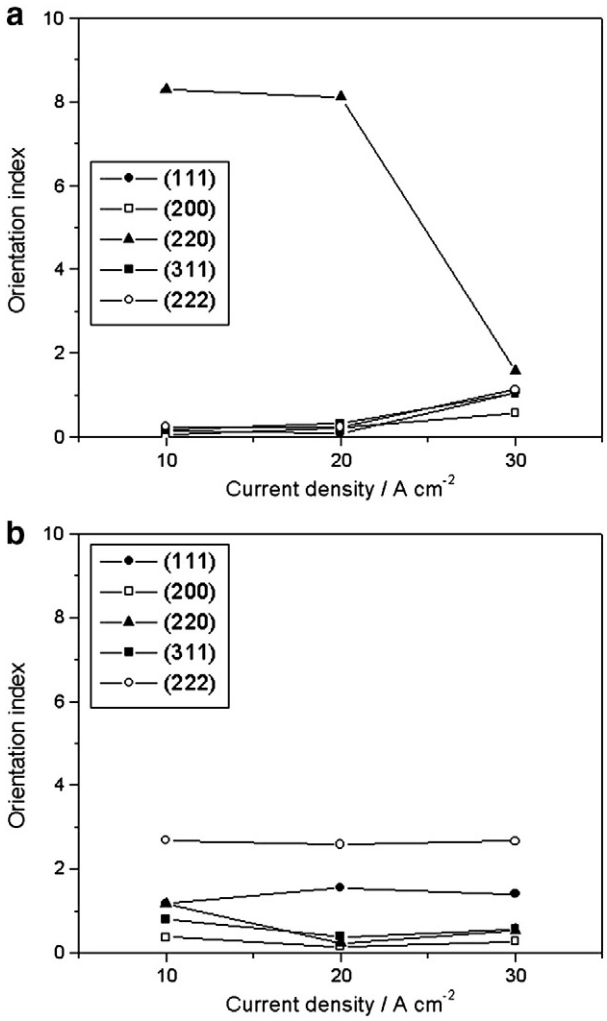

Fig. 9. Orientation index of the (111), (200), (220), (311) and (222) planes of the copper phase in (a) pure copper and (b) Cu–Si_3N_4 composite coatings obtained under the following conditions: (i) 10 $mAcm^{-2}$, 240 rpm, 50 gL^{-1}; (ii) 20 $mAcm^{-2}$, 400 rpm, 30 gL^{-1}; and (iii) 30 $mAcm^{-2}$, 240 rpm, 50 gL^{-1}.

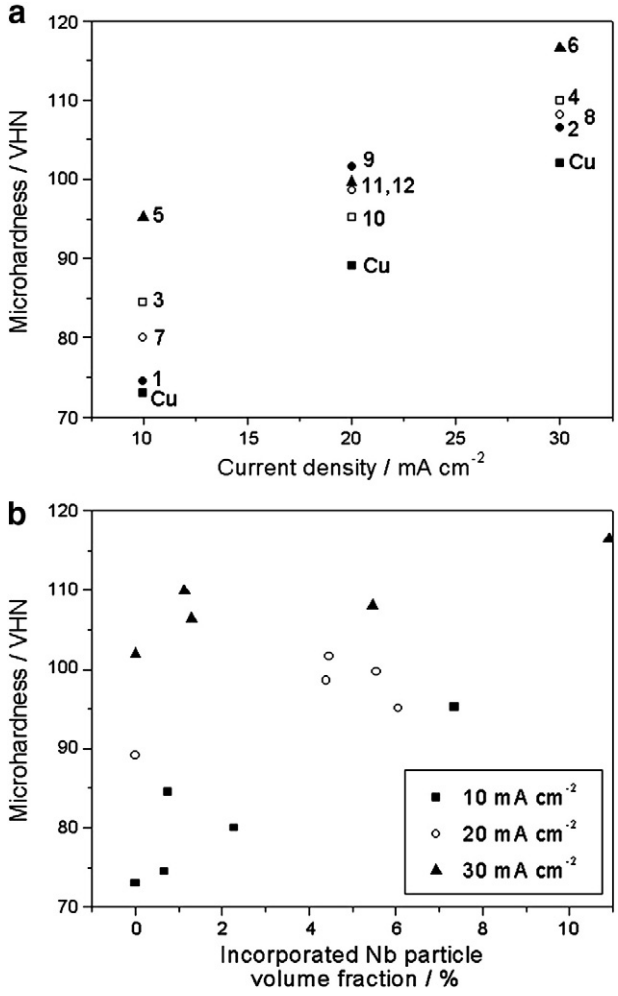

Fig. 10. Microhardness of pure copper and Cu–Nb composite coatings as a function of (a) cathodic current density and (b) incorporated Nb particle volume fraction.

composites was higher than that of pure copper. The increase in microhardness of pure copper coatings with increasing current density was attributed to copper grain refinement, due to a higher copper crystal nucleation rate [28]. Comparing composite coatings with nearly the same Nb particle content (for example, nearly 1% for experiments 1, 2, 3 and 4 or nearly 5% for experiments 8 and 11), the deposits obtained using 30 $mAcm^{-2}$ (experiments 2, 4 and 8) have higher microhardness than those obtained using 10 $mAcm^{-2}$ (experiments 1, 3 and 11). This proves that a reduction of the copper matrix grain size also occurred for the composites with increasing current density.

At constant current density, microhardness increases with increasing of the incorporated Nb particle content (Fig. 10b). Particle-strengthening which is related to the incorporation of hard particles and volume fraction above 20%, as well as dispersion-strengthening which is associated to the incorporation of fine particles (<1 μm) and volume fraction lower than 15% [29] cannot explain the higher microhardness of composites when compared to that of pure copper coatings. The matrix grain refining due to the nucleation of small grains on the surface of the incorporated Nb particles, resulting in a general structural refinement, is probably responsible for the higher microhardness of composites. The matrix copper grain refinement was observed in Cu–CeO_2 [12] and Cu–SiC [17] composites. The incorporation of SiC [6,17], Al_2O_3 [6,7], CeO_2 [12] and ZrB_2 [15] particles also led to an increase in microhardness when compared to that of pure copper.

Table 3
Corrosion potential, corrosion current density and polarization resistance of pure copper and Cu–Nb composite coatings (obtained using 30 $mAcm^{-2}$) in 0.5 wt.% H_2SO_4 solution at room temperature.

	Cu	Cu-1.3% Nb	Cu-5.4% Nb	Cu-10.9% Nb	Nb
Corrosion potential (V/SCE)	−0.084	−0.116	−0.146	−0.216	−0.263
Corrosion current density (μAcm^{-2})	10.1	8.5	5.0	4.3	2.5
Polarization resistance (kΩcm^2)	2.3	2.7	5.3	7.2	92.0

3.3. Corrosion behavior

The corrosion potential of Cu–Nb composite electrocoatings (obtained using 30 mA cm^{-2} deposition current density) measured after 1 h immersion in 0.5 wt.% H_2SO_4 solution ranged between the values obtained for copper deposit and commercially pure niobium, −0.084 and −0.263 V/SCE, respectively (Table 3). The corrosion potential of the composites shifted in the negative direction as the Nb content increased. In the same solution, Benea [11] measured corrosion potentials of −0.107 and −0.134 V/SCE for pure copper and Cu–ZrO_2 composite electrocoatings, respectively.

The shapes of the polarization curves of both pure copper and Cu–Nb composite coatings (Fig. 11) are very similar which shows that the anodic and cathodic reactions occurring on both surfaces are identical. The anodic dissolution of copper in sulfuric acid occurs in two steps [30,31] according to:

$$Cu \rightarrow Cu(I)_{ads} + e \quad (5)$$

and

$$Cu(I)_{ads} \rightarrow Cu^{2+} + e \quad (6)$$

where $Cu(I)_{ads}$ is an adsorbed Cu(I) species or Cu_2O compound.

The anodic curve for niobium is characteristic of passive materials.

The cathodic reactions in naturally aerated solutions are due to oxygen reduction close to the null-current potential, followed by H_2 evolution at more negative potentials according to [32]:

$$O_2 + 4H^+ + 4e \rightarrow 2H_2O(\text{acid solution}) \quad (7)$$

$$\text{or } O_2 + 2H_2O + 4e \rightarrow 4OH^-(\text{neutral and basic solution}) \quad (8)$$

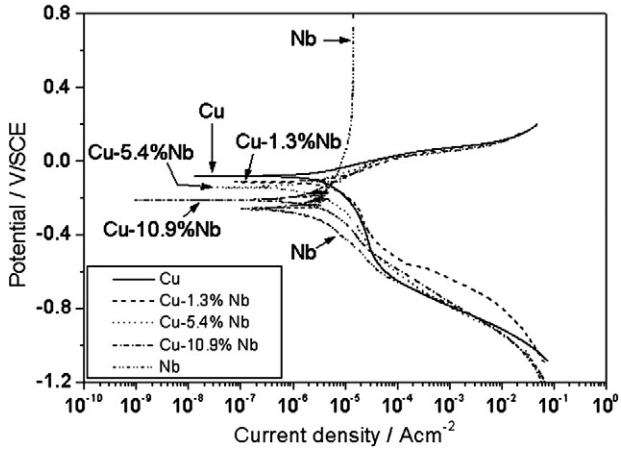

Fig. 11. Polarization curves recorded in 0.5 wt.% H_2SO_4 solution at room temperature for commercially pure Nb, pure copper and Cu–Nb composite coatings obtained under the following conditions: (Cu) 30 $mAcm^{-2}$; (Cu-1.3%Nb) 30 $mAcm^{-2}$, 240 rpm, 10 gL^{-1}; (Cu-5.4%Nb) 30 $mAcm^{-2}$, 550 rpm, 50 gL^{-1}; and (Cu-10.9%Nb) 30 $mAcm^{-2}$, 240 rpm, 50 gL^{-1}.

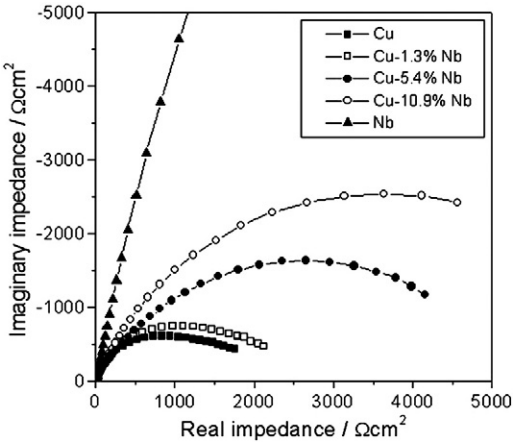

Fig. 12. Nyquist impedance diagram recorded at corrosion potential in 0.5 wt.% H_2SO_4 solution at room temperature for commercially pure Nb, pure copper and Cu–Nb composite coatings obtained under the following conditions: (Cu) 30 $mAcm^{-2}$; (Cu-1.3%Nb) 30 $mAcm^{-2}$, 240 rpm, 10 gL^{-1}; (Cu-5.4%Nb) 30 $mAcm^{-2}$, 550 rpm, 50 gL^{-1}; and (Cu-10.9%Nb) 30 $mAcm^{-2}$, 240 rpm, 50 gL^{-1}.

$$\text{and } 2H^+ + 2e \rightarrow H_2 \text{(acid solution)} \quad (9)$$

$$\text{or } 2H_2O + 2e \rightarrow H_2 + 2OH^- \text{(neutral and basic solution)} \quad (10)$$

respectively. In our case (H_2SO_4 solution) reactions (7) and (9) occurred.

Table 3 shows the corrosion current density of both pure copper and composite coatings determined by the extrapolation method. The value obtained for niobium was also reported for comparison purpose. The incorporation of Nb particles led to an improvement of corrosion resistance and the corrosion resistance increased as the Nb content increased. The impedance data confirmed this behavior. The impedance spectra presented on the Nyquist diagram (Fig. 12) display depressed capacitive semi-circles whose size increases with the increase of the Nb particle content. The corrosion resistance of copper and Cu–Nb composites was determined by the polarization resistance Rp, which can be obtained by:

$$Rp = \lim_{\omega \to 0} Z_{real} \quad (11)$$

where Z_{real} is the real part of impedance and ω is the angular frequency ($=2\pi f$, where f is the frequency in Hz). The values of Rp are reported in Table 3. The polarization resistance increases with the increase of the Nb particle content, which indicates an increase in corrosion resistance. Since Nb intrinsically presents a higher corrosion resistance than Cu in most aqueous media [32], it is expected that the incorporation of Nb particles in copper produces more corrosion-resistant coatings. On the other hand, the incorporation of Nb particles decreases the copper matrix grain size, which should lead to a decrease in corrosion resistance [33]. Thus, the slightly higher resistance of the composite coatings when compared to the pure copper layer suggests that the effect of incorporation of highly corrosion-resistant particles is predominant.

4. Conclusions

Well-crystallized Cu–Nb composite electrocoatings with uniform Nb particle distribution were obtained on carbon steel by electrolysis of an acidic sulfate bath containing suspended Nb particles.

The composite coatings were rougher than pure copper layers and their roughness increased with the increase of current density due to nodular growth.

The growth of the copper matrix was perturbed by the incorporation of Nb particles and the copper grains grew with random orientation.

Using DOE (Design of Experiments) Nb particle concentration in the bath was shown to be the most significant factor for the incorporation of Nb particles in copper, followed by stirring rate. Current density presented low significance. Under our experimental conditions, the highest Nb particle concentration, the lowest stirring rate and the highest current density led to the largest amount of incorporated Nb particles.

The microhardness of the composite coatings was higher than that of pure copper due to copper matrix grain refinement and increased with the increase of both cathodic current density and incorporated Nb particle content.

The corrosion resistance of Cu–Nb composites in 0.5 wt.% H_2SO_4 solution at room temperature was slightly higher than that of pure copper and increased with the increase of the Nb particle content.

Acknowledgment

A. Robin acknowledges CNPq (National Council for Development and Research — Brazil) for financial support (proc. 473131/2007-2).

References

[1] A. Hovestad, L.J.J. Janssen, J. Appl. Electrochem. 25 (1995) 519.
[2] M. Musiani, Electrochim. Acta 45 (2000) 3397.
[3] J.P. Celis, J.R. Roos, J. Electrochem. Soc. 124 (1977) 1508.
[4] C. Buelens, J.P. Celis, J.R. Roos, J. Appl. Electrochem. 13 (1983) 541.
[5] H. Hayashi, S. Izumi, I. Tari, J. Electrochem. Soc. 140 (1993) 362.
[6] V.D. Stankovic, M. Gojo, Surf. Coat. Technol. 81 (1996) 225.
[7] Y.L. Wang, Y.Z. Wan, Sh.M. Zhao, H.M. Tao, X.H. Dong, Surf. Coat. Technol. 106 (1998) 162.
[8] Y.X. Gan, C.S. Wei, M. Lam, X. Wei, D. Lee, J.W. Kysar, X. Chen, J. Mater. Sci. 42 (2007) 5256.
[9] I.A. Abdullin, R.S. Saifullin, Prot. Met. 33 (1997) 196.
[10] V. Medeliene, R. Juskenas, M. Kurtinaitiene, M. Jaskula, Pol. J. Chem. 78 (2004) 1305.
[11] L. Benea, O. Mitoseriu, J. Galland, F. Wenger, P. Ponthiaux, Mater. Corros. 51 (2000) 491.
[12] V. Mangam, K. Das, S. Das, Mater. Chem. Phys. 120 (2010) 631.
[13] V. Medeliene, M. Kurtinaitiene, G. Bikulcius, V. Stankevic, Surf. Coat. Technol. 200 (2006) 6123.
[14] Z.J. Jin, M. Zhang, D.M. Guo, R.K. Kang, Key Eng. Mater. 291–292 (2005) 537.
[15] D.M. Guo, M. Zhang, Z.J. Jin, R.K. Kang, J. Mater. Sci. Technol. 22 (2006) 514.
[16] J.G. Tang, K. Hu, S.H. Fu, H.J. Qi, Z.S. Jia, K. Li, H.K. Pang, F.H. Wang, J. Appl. Polym. Sci. 69 (1998) 1159.
[17] J. Zhu, L. Liu, G. Hu, B. Shen, W. Hu, W. Ding, Mater. Lett. 58 (2004) 1634.
[18] D. Thiemig, R. Lange, A. Bund, Electrochim. Acta 52 (2007) 7362.
[19] V. Medeliene, A. Kosenko, Mater. Sci. 14 (2008) 29.
[20] F. Heisterkamp, T. Carneiro, Niobium: Future possibilities- Technology and the market place, Science and Technology, TMS, Warrendale, Niobium, 2003.
[21] H.R.Z. Sandim, Preparation of Nb-TiO_2 alloys by powder metallurgy and its microstructural characterization, PhD Thesis, University of São Paulo, 1996.
[22] Selected Powder Diffraction Data – Metals and Alloys, Data Book, JCPDS International Centre for Diffraction Data, Swarthmore, 1978.
[23] D.C. Montgomery, Design and Analysis of Experiments, John Wiley & Sons, New York, 2005.
[24] P.J. Ross, Taguchi Techniques for Quality Engineering, McGraw-Hill, New York, 1996.
[25] P. Berçot, E. Pena-Munoz, J. Pagetti, Surf. Coat. Technol. 157 (2002) 282.
[26] K.S. Willson, J.A. Rogers, J. Tech. Proc. Amer. Electroplaters. Soc. 51 (1964) 92.
[27] A. Robin, J.C.P. de Santana, A.F. Sartori, J. Appl. Electrochem. 40 (2010) 507.
[28] W.H. Safranek, The Properties of Electrodeposited Metals and Alloys, Elsevier, Amsterdam, 1974.
[29] I. Garcia, J. Fransaer, J.P. Celis, Surf. Coat. Technol. 148 (2001) 171.
[30] H. Ma, S. Chen, B. Yin, S. Zhao, X. Liu, Corros. Sci. 45 (2003) 867.
[31] G. Quartarone, T. Bellomi, A. Zingales, Corros. Sci. 45 (2003) 715.
[32] ASM Handbook, Corrosion, Vol. 13, ASM International, Materials Park, 1992.
[33] J.W. Dini, Electrodeposition: The Materials Science of Coatings and Substrates, Noyes Publications, New Jersey, 1993.